Jupiter and Saturn as Spectral Analogs for Extrasolar Gas Giants and Brown Dwarfs: Bridging the Gap Between the Solar System and Exoplanets

A Thesis

Presented in Partial Fulfillment of the Requirements for the

Degree of Master of Science

with a

Major in Physics

in the

College of Graduate Studies

University of Idaho

by

Daniel J. Coulter

Approved by:

Major Professor: Jason W. Barnes, Ph.D.

Committee Members: Matthew M. Hedman, Ph.D.; Christine A. Berven, Ph.D.

Department Administrator: John R. Hiller, Ph.D.

May 2022

Abstract

With recent developments in direct imaging spectroscopy, the exoplanet community will soon have access to the spectra of hundreds, or even thousands, of extrasolar gas giants and brown dwarfs. However, as point-source spectra, there will be no spatially resolved context for these observations. In this thesis, I discuss using Jupiter and Saturn, our only spatially resolvable counterparts to extrasolar gas giants and brown dwarfs, as spectral analogs. In Chapter 1, I provide a brief historical context for this thesis and discuss its motivation and impact. In Chapter 2, I present point-source spectra of Jupiter and Saturn for a variety of phase angles, as well as provide end member, or single-feature spectra, for permutations of illumination and cloud density. Here, I also briefly touch on using spectral variations as a means to detect rings around exoplanets. Finally, in Chapter 3, I discuss future projects that are extensions of the work presented in this thesis.

Acknowledgments

Based on an admittedly small sample size, it seems like this is where the author thanks no less than a dozen people who were crucial in the success of their thesis. Because of the nature of this project and the restrictions on travel and collaboration due to Covid-19 (which nearly perfectly coincided with the bulk of work on this project), this list is quite small in my case. Nevertheless, there were five individuals without which this thesis would have been impossible (or at least far more difficult).

There is no one that deserves more acknowledgment than my advisor, Dr. Jason Barnes. Primarily performing research in atomic physics as an undergrad (with some dabbling in observational stellar astronomy) and deciding to switch fields for graduate school, I was definitely at an experiential disadvantage. When no other graduate program was willing to give me a chance, Jason welcomed me to the University of Idaho and into his research group with open arms, allowing me to continue my education while making the switch to planetary science. I appreciate his trust in my ability to perform the required research without micromanagement and also his willingness to help me when I hit those unavoidable roadblocks all graduate students encounter. Finally, I would like to thank him for his support as I transition from academia to a career in high school teaching, which I hope will be a long and rewarding one. Without him this thesis would not have been even remotely possible.

I would also like to thank my other coauthor, Dr. Jonathan Fortney. As the atmospheric modeling expert on the author list, he provided much needed context for this study and improved the final paper greatly. Since we never got to meet in person, I am taking this chance to formally thank you for your help.

Next, I would like to thank my other committee members, Dr. Matt Hedman and Dr. Christine Berven, for taking the time out of their busy schedules to serve on my committee.

Finally, I would like to thank my fellow graduate student Michael Heslar for all his help with anything VIMS cube related. Most importantly, he so graciously answered many of my dumb questions, meaning I didn't have to bother Jason nearly as much, which I am sure Jason also greatly appreciates. He also provided a way for me to convert VIMS cubes from the hot mess of a data structure they are into a much more orderly csv format. This allowed me to work in my native language of Python and avoid C++ altogether. Many headaches were avoided thanks to Michael.

Dedication

To my parents, Jim and Michelle - who so selflessly raised me to be the person I am today. I could never thank you enough. By this point you probably expected me to have a lucrative job making the big bucks, allowing you to retire in style. Better yet, you got this thesis,

To my high school physics teacher, John Plough - who instilled in me a love for physics. Without you I probably would have ended up studying engineering,

To my former research advisors, Jaideep Singh and Laura Chomiuk - who, to my bewilderment, actually took a chance on me as an undergrad and taught me the skills needed to succeed in graduate school,

And to my fellow peakbaggers; Mark Adrian, John Hamann, Terri Rowe, Richard Perkins, Ben Baumann, Richard Hensley, and many others - who are all such wholesome people and so warmly invited me into the community. May we climb many more mountains together,

"I shall be telling this with a sigh
Somewhere ages and ages hence:
Two roads diverged in a wood, and I–
I took the one less traveled by,
And that has made all the difference."
-Robert Frost

Table of Contents

Abstract . . . ii
Acknowledgements . . . iii
Dedication . . . iv
Table of Contents . . . v
List of Tables . . . vi
List of Figures . . . vii
Chapter 1: Introduction . . . 1
Historical Background . . . 1
Motivation and Impact . . . 2
Chapter 2: Jupiter and Saturn as Spectral Analogs for Extrasolar Gas Giants and Brown Dwarfs . . . 4
Abstract . . . 4
Introduction . . . 4
Brown Dwarfs and Gas Giants . . . 4
Direct Imaging Spectroscopy . . . 5
Observations & Methods . . . 6
Cassini VIMS Observations . . . 6
Data Reduction . . . 8
Disk-Integrated Spectra . . . 9
End Member Spectra . . . 9
Signal to Noise Ratio Calculation . . . 11
Jupiter . . . 11
Results . . . 11
Discussion . . . 12
Saturn . . . 15
Results . . . 15
Discussion . . . 15
Conclusions . . . 18
Chapter 3: Conclusions . . . 20
References . . . 22

List of Tables

2.1 VIMS spectral cubes selected for this study. All data presented here were retrieved from the NASA Planetary Data System (PDS) archive, except the resolution values marked with an asterisk, which were not available in PDS and we calculated ourselves. 7

List of Figures

2.1 Visual representation of the four end members outlined in Section 2.3.4. Incident solar light (white) can either be reflected by dense clouds (green) or cloudless regions (orange). Thermal emission (red) are either directly emitted or scattered by cloud layers (blue). 10

2.2 Signal to noise ratio as a function of wavelength for both Jupiter and Saturn. As expected, the signal to noise ratio is very low in the major absorption bands. The data used to generate this figure can be found in the supplementary information. 12

2.3 *Top*: Disk-integrated spectra of Jupiter in units of flux for six phase angles ranging from 1.7° to 133.5°. *Bottom*: Same as above, but in units of I/F. Prominent absorption bands are labelled. Absorption bands in the visual and infrared wavelengths are taken from [Vdovichenko et al., 2021] and [Baines et al., 2005], respectively. The source data for this figure can be found in the supplementary information. 13

2.4 Jupiter end member spectra obtained from cube V1357335218_1 (see Figure 2.5). The data used to generate this figure can be found in the supplementary information. 14

2.5 Color image of Jupiter (cube V1357335218_1) with green mapped to 2.0 μm, red mapped to 5.0 μm, and blue mapped to 2.4 μm. In this color scheme, green represents reflected light, red represents thermal emission, and blue indicates the presence of water ice. Note the lack of blue in this image in comparison to Figure 2.8, in which Saturn's rings, primarily composed of water ice, are clearly visible in blue. 14

2.6 *Top*: Disk-integrated spectra of Saturn in units of flux for four phase angles ranging from 39.6° to 110.2°. Due to the nature of Cassini's orbit around Saturn, full disk, full phase spectra were impossible to obtain. *Bottom*: Same as above, but in units of I/F. Once again, prominent absorption bands, courtesy of [Vdovichenko et al., 2021] and [Baines et al., 2005], are labelled. The data used to generate this figure, as well as for two additional phase angles, can be found in the supplementary information. 16

2.7 *Top*: Saturn end member spectra obtained from cube V1469259344_1 (see Figure 2.8). *Bottom*: Same as above but the y-scale has been adjusted to show detail. The features in the nightside spectra in the visible wavelengths are evidence of ringshine from Saturn's rings. The data used to generate this figure can be found in the supplementary information. 17

2.8 Color image of Saturn (cube V1469259344_1) with the same color mapping as in Figure 2.5: green to 2.0 μm, red to 5.0 μm, and blue to 2.4 μm. 17

2.9 Spectral comparison of two ring geometries: edge-on rings from cube V1518276136_1 (green) and rings at an inclination of approximately 20° from cube V1469259344_1 (magenta). Spectra with the rings and their shadows removed are shown for comparison. 18

Chapter 1: Introduction

1.1 Historical Background

The study of exoplanets, defined as planets beyond our solar system, is a surprisingly recent addition to the field of astronomy. By the most common definition, the study of exoplanets was born after the discovery of 51 Pegasi b, the first exoplanet found orbiting a main sequence star, in 1995 [Mayor and Queloz, 1995]. This just so happens to be the year I was born, and for the first nine months of my life the field in which I am now publishing my thesis did not really exist, making the progress in the field even more impressive.

After the discovery of 51 Pegasi b, a field which had been floundering in obscurity had now been reinvigorated. Detection of new exoplanets in the 1990s and 2000s was done primarily with the radial velocity method, in which the redshift and blueshift of stars due to the gravitational influence of an orbiting planet is measured. Progress was slow, however, due to the extreme precision required and the radial velocity method's bias toward very large planets orbiting near their host star (known as Hot Jupiters) in a nearly edge-on orientation as viewed from Earth. During this time several other detection methods were developed, foremost of which were the transit method, gravitational microlensing, and direct imaging. The transit method, in which the change in brightness of a star is measured as a planet passes in front of it, quickly became the most common method of detecting exoplanets, due to in no small part the *Kepler Space Telescope*. Entering service in 2009, the *Kepler Space Telescope* continuously observed a small portion of the sky until its decommissioning in 2018, hoping to observe transits of planets orbiting some of the stars in its field of view. To date, the *Kepler Space Telescope* has detected over 3600 exoplanets, with more being announced every year. In fact, over 70% of all known exoplanets were discovered by the Kepler Space Telescope, making it the single most important advancement in the field.

Despite the success of the transit method, it shares many of its biases with the radial velocity method, primarily that it requires a short-period orbit and an edge-on orientation of the exoplanet system. In addition, both methods are indirect methods, meaning the presence of a planet is inferred from measurements of its host star and not of the planet itself. Therefore, spectra of the planets cannot be acquired from these methods, making meaningful characterization impossible. With the focus of exoplanet research shifting from detection to characterization, a new technique was ready to take center stage: direct imaging. While technically challenging, direct imaging remedies nearly all of the problems of the radial velocity and transit methods. It is not biased to any particular orientation and is biases toward long-period orbits, which fills in a huge gap left by the other methods. And most importantly, as its name

suggests, it is a direct detection method, so spectra of the planet can be obtained and used for characterization. To date, only 58 exoplanets have been discovered by direct imaging, but it is no doubt the future of the field. The next generation of space telescopes, including the *James Webb Space Telescope* (JWST) and the *Nancy Grace Roman Space Telescope* (formerly WFIRST), are fitted with coronagraphs, enabling them to directly image exoplanets. In addition, two NASA concept missions, *HabEx* and *LUVOIR*, both have science goals of directly imaging and characterizing exoplanets.

1.2 Motivation and Impact

Currently, the planetary science field is split into two distinct camps: those that study the solar system planets and those that study exoplanets and brown dwarfs. There is surprisingly little overlap between these two communities, but it is not completely unexpected. For one, humans have been studying the solar system planets in some way or another since antiquity, and there is a rich heritage in this community. On the other hand, those of us that study exoplanets are very much the new kids on the block. These two communities have also historically had access to very different data sets. The solar system community has access to only two gaseous planets, Jupiter and Saturn, but they have both been studied in excruciating detail by NASA missions for decades. In contrast, the exoplanet community has access to thousands of planets, but only has a rudimentary knowledge of any single one. This makes the solar system community well-positioned to describe a very specific type of planet, but unable to make any declarations beyond that. Meanwhile, the exoplanet community is better suited to describe planets from a statistical perspective, but cannot provide significant insight into specific exoplanets. At first, these data sets appear to compliment each other nicely, but it is not that simple. Most exoplanets discovered to date are large gaseous planets orbiting very near their host star, often much closer than Mercury to the Sun. Therefore, they do not have a solar system analog, making comparisons difficult. However, this paradigm is rapidly shifting as we conquer the technical limitations of the previous era of telescopes. With the advent of direct imaging we can now observe gaseous planets far from their host stars, and we have pushed the limits to detect cooler and cooler brown dwarfs. With each advancement, the solar system and exoplanet communities are drawn closer and closer together.

The motivation behind this thesis is to help bridge the gap between the solar system and exoplanet communities. One of the main objectives of the exoplanet community is to characterize the dynamic atmospheres of extrasolar gas giants and brown dwarfs, but at the distances they reside, they are unresolvable point sources. Any spectra obtained from exoplanets and brown dwarfs is necessarily of the entire body and shows no direct detail of weather patterns. Therefore, the community has resorted to

using models based on temporal changes to the planet-wide spectra. However, without ground truth test cases the validity of the models is unclear. Thankfully, the solar system community has provided millions of beautiful resolved images of two gas giants, Jupiter and Saturn, to aid in validate these models. In this thesis, I present disk-integrated spectra of Jupiter and Saturn obtained from spectral cubes from the *Cassini* Visual and Infrared Mapping Spectrometer (VIMS) instrument. These spectra will act as an analog to the point source spectra obtained from extrasolar gas giants and brown dwarfs, while also having spatially resolved source images to validate models.

As the purpose of this project is to bridge the gap between the solar system and exoplanet communities, its impact aims to benefit both communities. Naturally, the data presented here is primarily of interest to the exoplanet atmosphere modelers, as it will compensate for the lack of resolved images of extrasolar gas giants and brown dwarfs. The ability for modelers to validate their models is undoubtedly a benefit to the exoplanet community. However, the work done by the exoplanet community will help answer many of the questions that persist in the solar system community. By understanding the nature of thousands of extrasolar gas giants and brown dwarfs, Jupiter and Saturn will be put into an extrasolar context, answering the question of whether Jupiter and Saturn are archetypal planets or unique. And with a wide age range represented in those thousands of exoplanets and brown dwarfs, planetary evolution can also be probed. Work done by the exoplanet community will also inform the solar system community where Jupiter and Saturn sit along the evolutionary path, a task impossible with only a sample of two similarly aged planets. And perhaps most importantly, this study and many other similar studies will promote communication between the communities and the sharing of data for the combined goal of understanding planets, both within our solar system and beyond it.

Chapter 2: Jupiter and Saturn as Spectral Analogs for Extrasolar Gas Giants and Brown Dwarfs

Daniel J. Coulter, Jason W. Barnes, Jonathan J, Fortney

Currently in review for publish in The Astrophysical Journal Supplement Series

2.1 Abstract

With the advent of direct imaging spectroscopy, the number of spectra from brown dwarfs and extrasolar gas giants is growing rapidly. Many brown dwarfs and extrasolar gas giants exhibit spectroscopic and photometric variability, which is likely the result of weather patterns. However, for the foreseeable future, point-source observations will be the only viable method to extract brown dwarf and exoplanet spectra. Models have been able to reproduce the observed variability, but ground truth observations are required to verify their results. To that end, we provide visual and near-infrared spectra of Jupiter and Saturn obtained from the *Cassini* VIMS instrument. We disk-integrate the VIMS spectral cubes to simulate the spectra of Jupiter and Saturn as if they were directly imaged exoplanets or brown dwarfs. We present six empirical disk-integrated spectra for both Jupiter and Saturn with phase coverage of 1.7° to 133.5° and 39.6° to 110.2°, respectively. To understand the constituents of these disk-integrated spectra, we also provide end member (single feature) spectra for permutations of illumination and cloud density, as well as for Saturn's rings. In tandem, these disk-integrated and end member spectra provide the ground truth needed to analyze point source spectra from extrasolar gas giants and brown dwarfs. Lastly, we discuss the impact that icy rings, such as Saturn's, have on disk-integrated spectra and consider the feasibility of inferring the presence of rings from direct imaging spectra.

2.2 Introduction

2.2.1 Brown Dwarfs and Gas Giants

Brown dwarfs are substellar objects that are not massive enough to sustain the fusion of hydrogen into helium but are massive enough to sustain deuterium fusion ($13 - 75$ M_J). Their temperatures range from over 2000 K for the hottest L-class brown dwarfs down to $\sim$ 250 K for the coldest Y-class

brown dwarf discovered to date [Luhman, 2014]. Due to their relatively low temperatures, brown dwarfs have atmospheres that allow for the condensation of molecules into clouds. Hot L-class brown dwarfs ($1300 - 2200$ K) have atmospheric spectra characterized by strong water vapor opacity, carbon dioxide, metallic hydrides, alkali metals, and optically think clouds thought to be composed of silicates and iron [Kirkpatrick et al., 1999]. For T-class brown dwarfs ($600 - 1300$ K), these signatures are dominated by prominent methane and water vapor absorption bands [Kirkpatrick et al., 1999, Burgasser et al., 2002]. One model for the L to T spectral class transition is marked by a shift from a largely uniform cloud layer to a mix of cloudy and cloudless regions, which eventually results in atmospheres potentially devoid of clouds [Burgasser et al., 2002, Marley et al., 2010], however this model is inconsistent with recent observations [Apai et al., 2013, Lew et al., 2020]. The spectra of cool Y-class brown dwarfs (less than 600 K) show even more pronounced methane and water absorption bands and the coolest members even show evidence of ammonia [Cushing et al., 2011]. Extrasolar gas giant planets cover this same temperature range, and are theorized to show similar atmospheric signatures [Sudarsky et al., 2000, Sudarsky et al., 2003, Fortney et al., 2020].

Since brown dwarfs do not generate energy from hydrogen fusion, their heat derives from gravitational contraction and is primarily in the form of thermal radiation, predominantly in the infrared. Clouds act as a barrier to this radiation, with patchy clouds yielding non-uniform emission signatures across the disk. Studies by [Crossfield et al., 2014] and [Metchev et al., 2015] suggest that photometric and spectral variability of brown dwarfs is the result of such patchy clouds. Similarly, Jupiter and Saturn radiate more energy than they receive from the Sun due to leftover heat from their formation [Aumann et al., 1969]. Photometric variations of brown dwarfs and gas giants, above and below the $13 - 75$ M_J boundary, are thought to be evidence of heterogeneous cloud distributions and atmospheric circulation [Zhou et al., 2016].

2.2.2 Direct Imaging Spectroscopy

Understanding how clouds form and evolve is a primary objective of brown dwarf and extrasolar gas giant research (see Question B3 in the white paper by [Apai et al., 2017]). Clouds are of first-order importance in these atmospheres, as they dramatically impact radiation transport and the atmospheric depth that one probes in spectral observations [Marley et al., 1999]. While brown dwarfs can typically be observed in isolation, without the bright glow of a parent star, this is not true for exoplanets. Progress in exoplanet atmosphere characterization via high-contrast imaging has been challenging due to technological limitations, but refined techniques and the next era of space telescopes show promise of significant progress

in the field. Recent reviews include [Traub and Oppenheimer, 2010] and [Biller and Bonnefoy, 2018].

There is a strong interest in the direct imaging and subsequent characterization of all varieties of exoplanets. The James Webb Space Telescope (JWST) and Nancy Grace Roman Space Telescope (formerly WFIRST) will be fitted with coronagraphs, which will enable direct imaging of exoplanets near bright stars. In addition, the Astro2020 decadal survey recommended a large ∼6-meter class space telescope with the driving science case to image and characterize exoplanets Earth-exoplanets with habitable zones of nearby Sunlike stars [National Academies of Sciences et al., 2021]. With the influx of direct imaging data expected in the coming decades, it is imperative that the exoplanet and brown dwarf communities are able to interpret this data using tools and modeling frameworks trained with ground truth observations from the solar system. Over the past several years, atmosphere models that aim to assess the temperature structure, composition, and reflection/emission spectra of directly imagined planets, as well as "retrieval" codes that aim to turn reflection spectra into atmospheric constraints, have been developed in anticipation of upcoming spectra [Lupu et al., 2016, Nayak et al., 2017, MacDonald et al., 2018, Damiano et al., 2020, Damiano and Hu, 2020].

Trying to assess the reflection and emission from solar system planets in the exoplanet context has expanded as well. Recently, [Gu et al., 2021] and [Simon et al., 2016] conducted spectral analysis studies of Earth and Neptune, respectively. Those studies provide solar system analogs for terrestrial planets and ice giants, but proxies for gas giants and brown dwarfs are still needed. Jupiter and Saturn, our only spatially resolvable comparison objects, act as a bridge between the point source spectra obtained from direct imaging and atmospheric models of brown dwarfs and gas giants.

In this paper we present visual and near infrared disk-integrated spectra of Jupiter and Saturn at various phase angles, defined hereafter as the sun-planet-*Cassini* angle. These spectra are proxies for point-source spectra of extrasolar gas giants obtained via direct imaging. We also present end member spectra for different combinations of illumination and cloudiness, which will be useful when attempting to deconstruct point-source spectra into constituent atmospheric features. Lastly, we discuss the ability to discern the presence of icy rings from point source spectra.

2.3 Observations & Methods

2.3.1 Cassini VIMS Observations

Spectral data comes from the *Cassini* Visual and Infrared Mapping Spectrometer (VIMS) instrument [Brown et al., 2004], which acquired individual point spectra with 352 spectral channels between 0.35 and

Target	Cube Name	Acquisition Date	VIS, IR Exposure (s)	Resolution (km/pixel)	Phase Angle (°)
Jupiter	V1355313318_3	2000 Dec 12	640, 20	9660	1.66
	V1353677179_2	2000 Nov 23	640, 20	17,478*	15.19
	V1357119162_1	2001 Jan 2	640, 20	5011	76.96
	V1357335218_1	2001 Jan 4	640, 20	5455	89.26
	V1357767306_1	2001 Jan 9	640, 20	6872	107.27
	V1359577908_1	2001 Jan 30	640, 20	15,536*	133.52
Saturn	V1564773481_1	2007 Aug 2	1280, 20	1862	39.64
	V1565414411_1	2007 Aug 10	1280, 20	2031	49.61
	V1565931915_1	2007 Aug 16	1280, 20	1883	57.76
	V1469259344_1	2004 Jul 23	1280, 120	3304	91.90
	V1518276136_1	2006 Feb 10	2560, 40	1925	101.07
	V1517685790_1	2006 Feb 3	2560, 40	1990	110.20

Table 2.1: VIMS spectral cubes selected for this study. All data presented here were retrieved from the NASA Planetary Data System (PDS) archive, except the resolution values marked with an asterisk, which were not available in PDS and we calculated ourselves.

5.2 μm. VIMS is composed of two separate optical and detector assemblies – the visual half, or VIMS-V, and the infrared half VIMS-IR – that employ a common pointing and spacecraft interface such that they operate as if they were a single instrument. Using a targeting mirror, VIMS was able to build spectral image cubes up to 64x64 pixels in size, providing adequate spatial resolution for this study. *Cassini* VIMS obtained over 14,000 cubes during its flyby of Jupiter and over 550,000 cubes of Saturn's disk during its 13 years in orbit. We compiled cubes suitable for this study based on three criteria:

(i) The image showed the entire disk of the target planet in order to obtain complete disk-integrated spectra

(ii) There were no pixels on the target planet's disk that were saturated due to overexposure

(iii) There were no objects or artifacts that would affect the spectra, such as a transiting moon or severe cosmic ray spikes

Under these constraints, the number of suitable cubes for both Jupiter and Saturn dropped to only a few dozen each, owing to the frequent overexposure of some wavelengths and the nature of *Cassini*'s orbit, which rarely allowed for full disk imaging of Saturn. These remaining cubes were clustered in groups of images taken in quick succession at similar phase angles, with many phase angles absent. Thus, full phase angle coverage is not possible without relaxing the selection criteria. In the end, six cubes each were selected for Jupiter and Saturn so that they provided the most complete phase angle coverage possible for each planet and for the two combined. The cubes selected for this study are shown in Table 2.1.

2.3.2 Data Reduction

We retrieved raw VIMS cubes from the NASA Planetary Data System (PDS) archive and reduced them using the pipeline described in [Barnes et al., 2013]. The processing proceeds as follows:

1. On-board the spacecraft, for each line VIMS observes it measures a background level. Raw cubes as downloaded from the spacecraft have the average value of this background measurement already subtracted from them. However since the on-board backgrounds have proven to be noisy, we first add the mean background back in to each pixel for the visual half of VIMS and the full measured background back in for the infrared half. Then for each cube we create a linear fit to the instrument-measured background observations acquired at the end of each row in the cube as a function of time and subtract the linearly interpolated background from each pixel. This method has proven to be much more robust against cosmic ray spikes and the slowly varying background level as compared to the on-board subtraction.

2. We begin the automatic pipeline process by marking those pixels that have saturated.

3. Next, the pipeline employs a despiking algorithm to identify pixels whose flux is dominated by cosmic ray hits. We assign the offending pixels an interpolated value based on a 3-D polynomial fit of the twenty-six nearest neighbor pixels. Results of the automated despiker compare favorably to manually despiked cubes for extended objects like Jupiter and Saturn, although the despike algorithm does incorrectly flag specular reflections off of Titan lakes as cosmic ray hits [Barnes et al., 2013].

4. We divide through by a spatial flatfield that was taken on the ground before launch at each wavelength. Lacking an instrumental mechanism for generating an in-flight flatfield, we tried using hundreds of uniformly illuminated science observation cubes to generate an empirical flatfield, but found the result inferior to the ground-based calibration.

5. We convert to specific energy (I_λ) using the instrument's spectro-radiometric response function $R(\lambda)$ in photons per analog-to-digital data number (DN) [Brown et al., 2004]:

$$I_\lambda = \frac{DN}{\tau} \times R(\lambda) \times \frac{hc}{\lambda} \times \frac{1}{A\Omega\delta\lambda} \tag{2.1}$$

where τ is the exposure time in seconds, h is Planck's constant, c is the speed of light, λ is the wavelength of this particular VIMS channel, $\delta\lambda$ is the size of the wavelength bin for this VIMS channel, A is the area of the VIMS mirror, and Ω is the solid angle subtended by a pixel in steradians.

6. Using SPICE [Acton, 1999] data provided by the NASA Jet Propulsion Laboratory (JPL), we calculate the latitude, longitude, x- and y-direction resolution, phase angle, incidence angle, emission angle, and north azimuth of every point individually. These data are stored in the cube backplane. Since VIMS is a spot-scanner [Brown et al., 2004], we are able to compensate for spacecraft pointing changes during an exposure. The SPICE geometry kernel files also contain knowledge of the spacecraft position relative to the target planet, which we ultimately use to convert observed specific energy into the net spectral flux of the planet.

This pipeline was specifically tailored for reducing cubes obtained during *Cassini*'s time orbiting Saturn. Therefore, the background subtraction in the visible wavelengths was not calibrated for Jupiter data and required an additional step in the data reduction process. To calibrate for visible wavelengths, we calculated the median value of the background (non-disk) pixels for each spectral band and then subtracted that value from all pixels in that band.

2.3.3 Disk-Integrated Spectra

Disk integration of Jupiter's spectral cubes was straightforward. For both spectral radiance and apparent reflectance (I/F), we simply coadded all pixels on the disk and divided by the number of pixels coadded. However, Saturn was more challenging, since information on the geometry of the rings is not present within the cube backplanes. Therefore, we manually masked out the pixels containing the rings and their shadows from the image. We replaced each missing pixel by swapping it with the pixel with the nearest incidence angle value. This process was done separately for VIMS-V and VIMS-IR since they had slightly different viewing geometries. Once the rings were synthetically removed from the images, we disk-integrated them as we did for Jupiter. Integrated images of Saturn with rings included were also produced and the comparison to the "ringless" Saturn is discussed in Section 2.5. This process provides spatially resolved examples of a planet with and without rings since some planets and brown dwarfs will host impressive ring systems while others will not.

2.3.4 End Member Spectra

We obtained end member, or single feature, spectra by selecting an individual pixel of the target feature and determining its radiance and apparent reflectance (I/F) values across all VIMS spectral channels, once again accounting for the difference in viewing geometry between VIMS-V and VIMS-IR. For each end member, we chose three such pixels and averaged them to reduce any noise present in a single pixel. Four end members are common to Jupiter and Saturn:

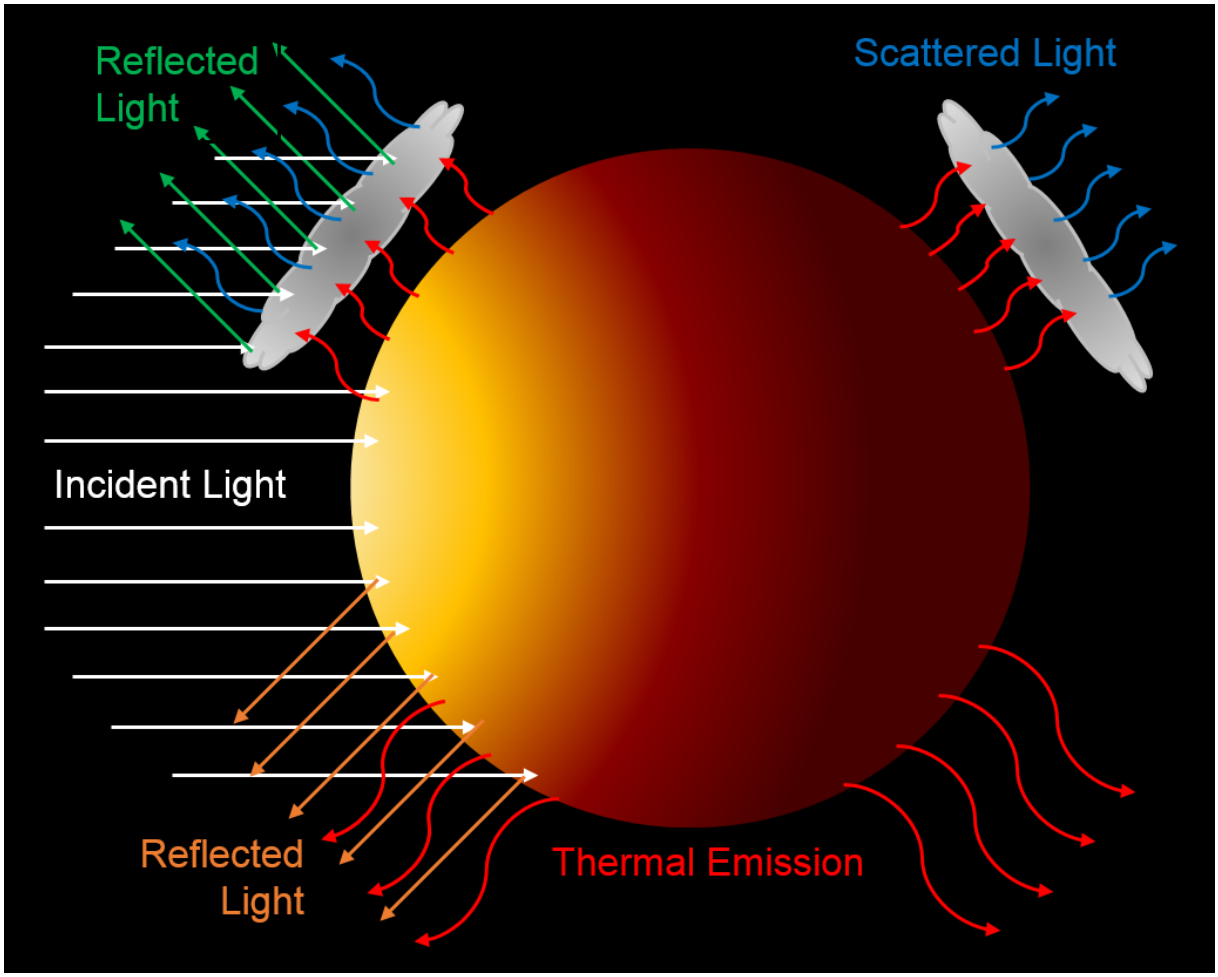

Figure 2.1: Visual representation of the four end members outlined in Section 2.3.4. Incident solar light (white) can either be reflected by dense clouds (green) or cloudless regions (orange). Thermal emission (red) are either directly emitted or scattered by cloud layers (blue).

1. **Dayside and Cloudy**: Regions that are on the illuminated area of the disk and have thick clouds that both reflect incident light and block thermal emission from the planet (upper left in Figure 2.1). On Jupiter, these are the cloud-dense zones on the illuminated side of the disk (bright green in Figure 2.5). On Saturn, this is the illuminated part of the cloudy region straddling its equator (yellow in Figure 2.8).

2. **Dayside and Clear**: Regions that are on the illuminated area of the disk and have few clouds to block thermal emission (lower left in Figure 2.1). On Jupiter, these are the cloud-free belts on the illuminated side of the disk (red on the illuminated side in Figure 2.5). On Saturn, this is the darker region just above the bright equatorial zone (reddish-brown in Figure 2.8).

3. **Nightside and Cloudy**: Regions that are on the dark side of the disk and have thick clouds that block thermal emission from the planet (upper right in Figure 2.1). On Jupiter, these are the cloud-dense zones on the dark side of the disk (black in Figure 2.5). On Saturn, this is the dark part of the cloudy region straddling its equator (red in Figure 2.8).

4. **Nightside and Clear**: Regions that are on the dark side of the disk and have fewer clouds to block thermal emission (lower right in Figure 2.1). On Jupiter, these are the belts on the dark side of the disk (red on the illuminated side in Figure 2.5), which have thinner clouds than the zones. On Saturn, this is the darker region just above the equatorial zone (dark red in Figure 2.8).

For Saturn, we produced two additional end member spectra for the A Ring and B Ring. All end member spectra from Jupiter and Saturn were obtained from cubes V1357335218_1 and V1469259344_1, respectively.

2.3.5 Signal to Noise Ratio Calculation

Uncertainties in the spectra are dominated by astrophysical aspects (i.e. angular position, small atmospheric variations) rather than instrumental ones. Therefore, viewing Jupiter or Saturn at the same phase angle, but at different times (thus different angular positions) will result in slightly different spectra. To account for these variations, we averaged the spectra of four nearby cubes for Jupiter and five such cubes for Saturn. The phase variations in these sets are 0.43° for Jupiter and 0.68° for Saturn. We calculated the means and standard deviations for both sets and divided the mean spectra by the standard deviation spectra (taken here to be the noise) to get a signal to noise ratio for both planets. Our results are shown in Figure 2.2.

2.4 Jupiter

2.4.1 Results

Disk-integrated spectra for six phase angles of Jupiter are shown in Figure 2.3. The visual and near infrared (below 3.5 μm) spectrum of Jupiter is dominated by reflected solar light with absorption bands primarily from methane (CH_4), phosphine (PH_3), and ammonia (NH_3). Of note is the ammonia absorption band at 3.0 μm, which is much more pronounced in Jupiter, leading to a single peak structure in the spectrum as opposed to the dual peak structure seen in Saturn (see Figure 2.6). Beyond 3.5 μm the influence of solar light wanes dramatically and the spectrum is now primarily thermal emission.

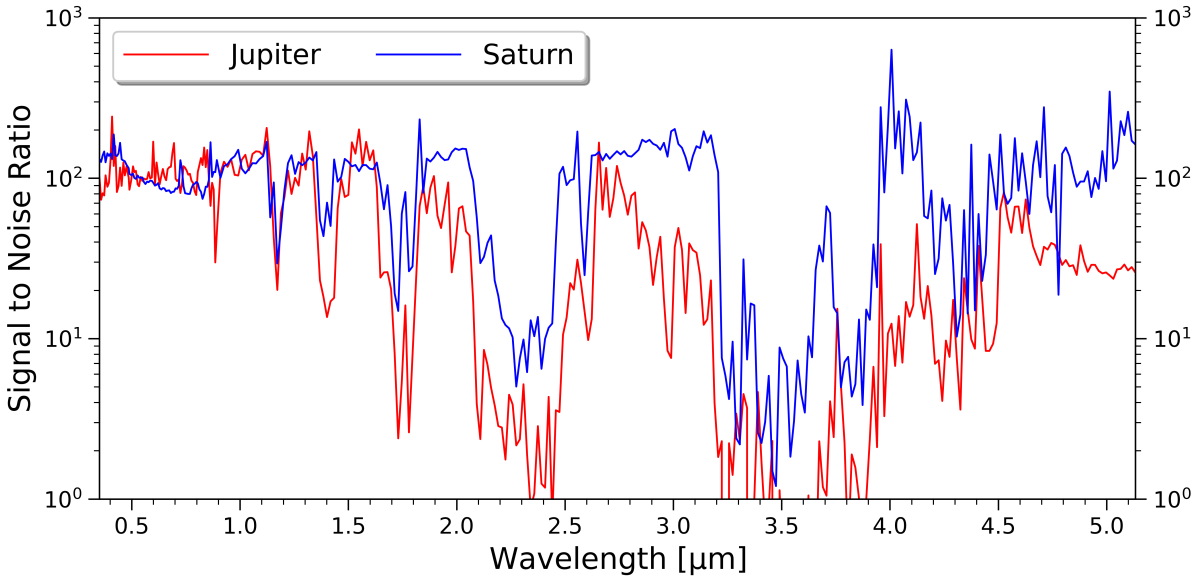

Figure 2.2: Signal to noise ratio as a function of wavelength for both Jupiter and Saturn. As expected, the signal to noise ratio is very low in the major absorption bands. The data used to generate this figure can be found in the supplementary information.

Therefore, the phase-dependent variations are no longer present in this regime. Despite the thermal radiation being minimal in comparison to reflected light in flux, it dominates the I/F spectrum (note the axis changes in both spectra of Figure 2.3).

Jupiter end member I/F spectra are shown in Figure 2.4. In the visual and near-infrared, both the dayside and nightside spectra are structurally similar, however their cloudy and clear members diverge dramatically in the mid-infrared. This dichotomy is the result of the extreme banding present in Jupiter's atmosphere, which can be seen visually in Figure 2.5. Jupiter's zones are particularly cloud-dense while the clouds are relatively sparse in their counterpart, the belts. The result is a significant percentage of thermal emission in zones are blocked, while thermal energy can more easily escape from belts. Beyond 4.5 μm, thermal emission dominates, so there should be no difference between the clear spectra (dashed lines in Figure 2.4) in this wavelength regime.

2.4.2 Discussion

Direct imaging requires that the target planet be further from the host star than other detection methods. Therefore, direct imaging spectroscopy is biased towards planets with modest incident fluxes, perhaps ∼1-5 AU. Planets as cool as Jupiter $T_{\text{eff}} = 125$K are dominated by gaseous methane and ammonia clouds [Sudarsky et al., 2000], so abundances of methane and other molecules can be determined by the

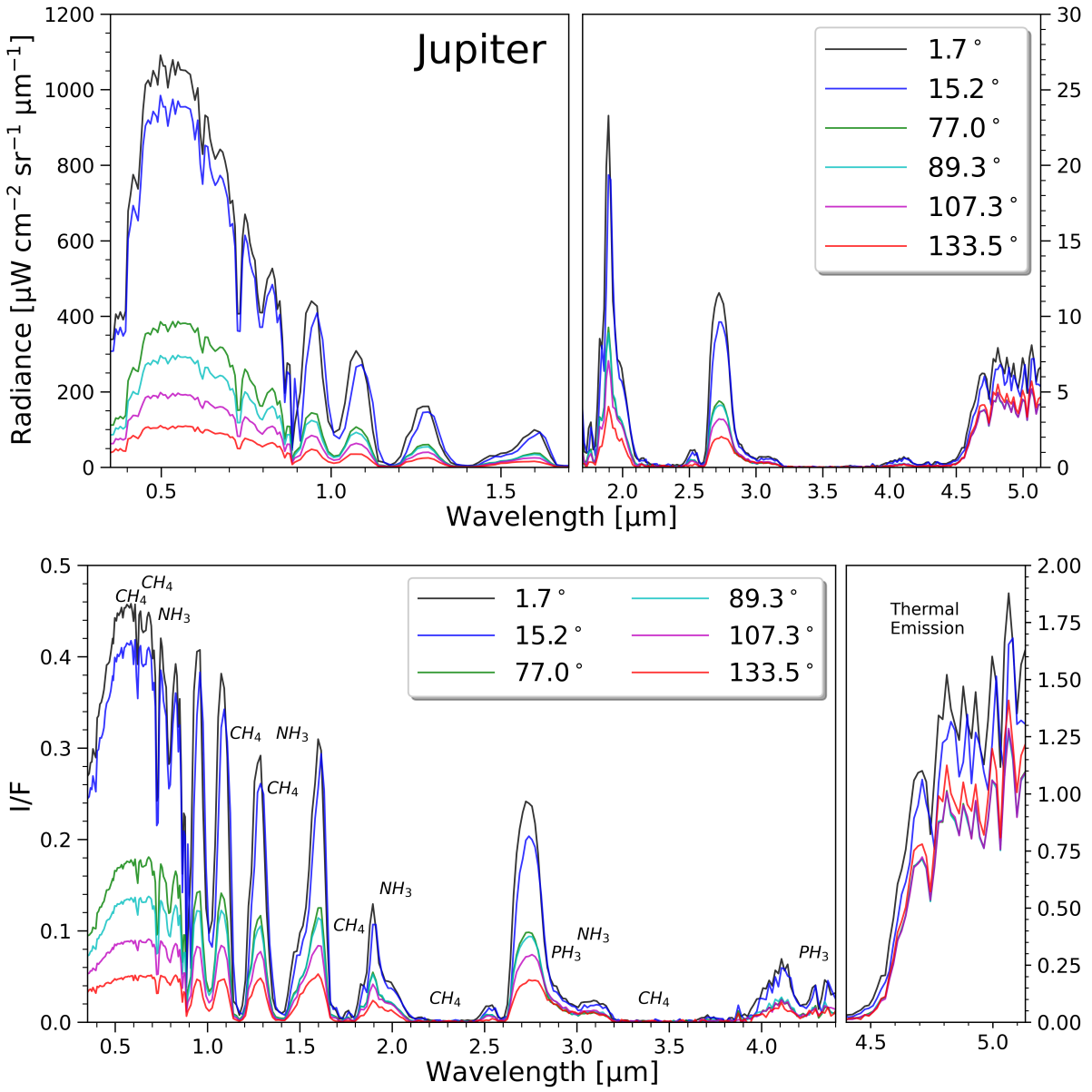

Figure 2.3: *Top*: Disk-integrated spectra of Jupiter in units of flux for six phase angles ranging from 1.7° to 133.5°. *Bottom*: Same as above, but in units of I/F. Prominent absorption bands are labelled. Absorption bands in the visual and infrared wavelengths are taken from [Vdovichenko et al., 2021] and [Baines et al., 2005], respectively. The source data for this figure can be found in the supplementary information.

depth of their absorption bands in reflection spectra. Therefore, future observing campaigns should have wavelength coverage and resolution to observe these absorption bands (e.g. the large methane bands centered on 2.3 μm and 3.5 μm and the ammonia band at 3.1 μm).

Since it emits thermal radiation, Jupiter also acts as a brown dwarf analog when viewed in the mid-

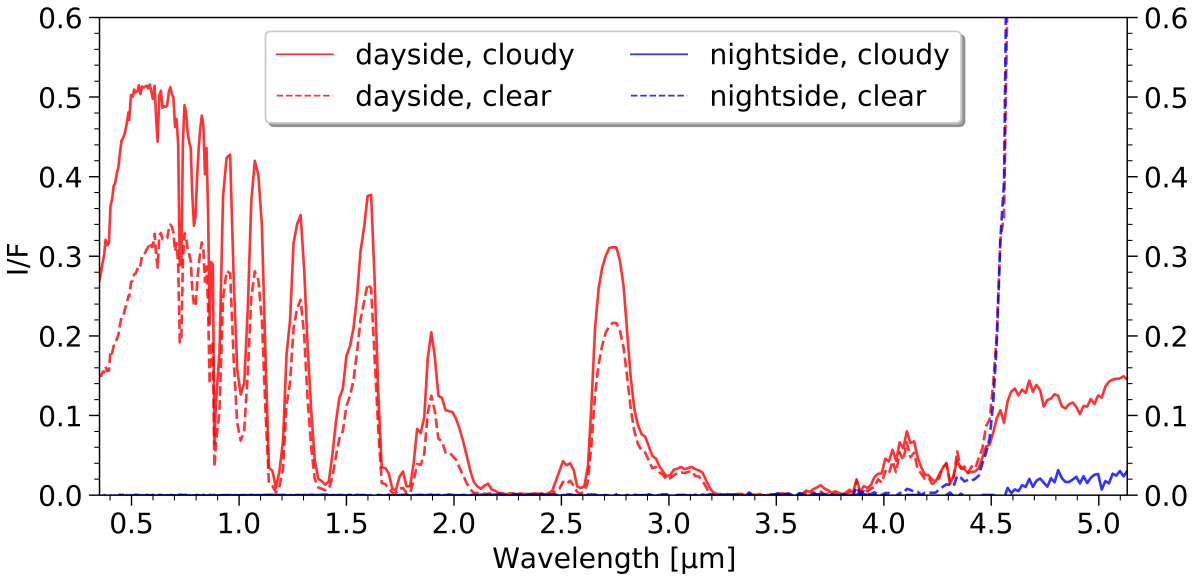

Figure 2.4: Jupiter end member spectra obtained from cube V1357335218_1 (see Figure 2.5). The data used to generate this figure can be found in the supplementary information.

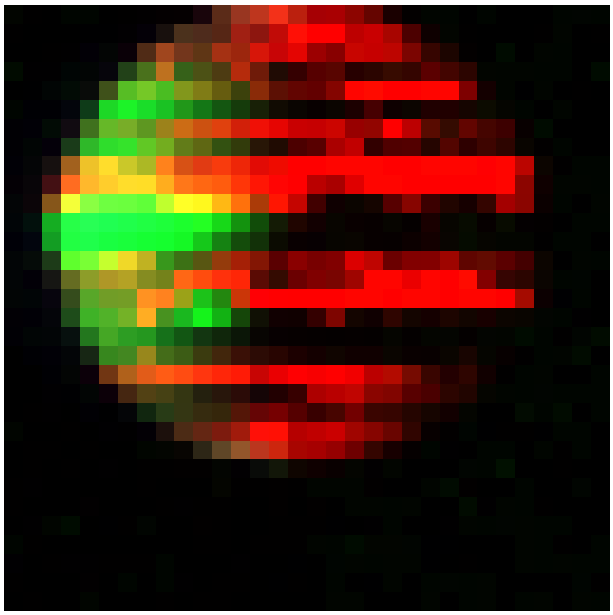

Figure 2.5: Color image of Jupiter (cube V1357335218_1) with green mapped to 2.0 μm, red mapped to 5.0 μm, and blue mapped to 2.4 μm. In this color scheme, green represents reflected light, red represents thermal emission, and blue indicates the presence of water ice. Note the lack of blue in this image in comparison to Figure 2.8, in which Saturn's rings, primarily composed of water ice, are clearly visible in blue.

infrared. Specifically, Jupiter is compositionally similar to ultra-cool Y-class brown dwarfs. As shown in Figure 2.3, this thermal emission is most prominent beyond 4.5 μm, where cool brown dwarfs are also known to be quite bright. Interestingly, the intensity of the thermal emission is highly dependent upon cloud density, which is apparent in Figure 2.4. Future brown dwarf observations can be be compared to the end member spectra presented here in order to constrain the relative amounts of cloudy and cloudless regions in their atmospheres.

2.5 Saturn

2.5.1 Results

Disk-integrated spectra for four phase angles of Saturn are shown in Figure 2.6. As with Jupiter, the visual and near-infrared spectrum is dominated by reflected light and many of the same methane, phosphine, and ammonia absorption bands, while the mid-infrared is dominated by thermal radiation. Owing to its more uniformly cloudy atmosphere, we do not see the same dramatic spike beyond 4.5 μm that we do in Jupiter's spectrum. This difference could potentially indicate the severity of banding of brown dwarfs and gas giants from point-source spectra alone. Saturn end member spectra are shown in Figure 2.7. Below 4.5 μm, the end members resemble those of Jupiter, but beyond 4.5 μm, we do not see the same wild divergence between cloudy and clear spectra. This lack of divergence in the infrared is once again the result of less severe banding in Saturn's atmosphere.

Composed almost entirely of water ice, Saturn's rings are compositionally different than Saturn itself. Water has few absorption bands in the visual and near-infrared, giving the A Ring and B Ring end member spectra a rather flat appearance in Figure 2.7. Therefore, the rings represent a minority share of the flux outside absorption bands, but are the contributing factor within them. This result illustrates the distinctive effect rings have on disk-integrated spectra and is expanded upon in the following section.

2.5.2 Discussion

Saturn, with its impressive ring system, provides an interesting test case for our ability to infer the presence of icy rings from point-source spectra alone. During its time in the Saturn system, *Cassini* observed Saturn from a range of orbital inclinations, from edge-on rings up to a 20° inclination. A comparison of edge-on and inclined ring spectra is shown in Figure 2.9. With edge-on rings, the spectrum shows little variation from its ringless counterpart. The slight decrease in the visual and near-infrared is the consequence of the rings casting shadows on the disk, resulting in less reflected light. In contrast, the

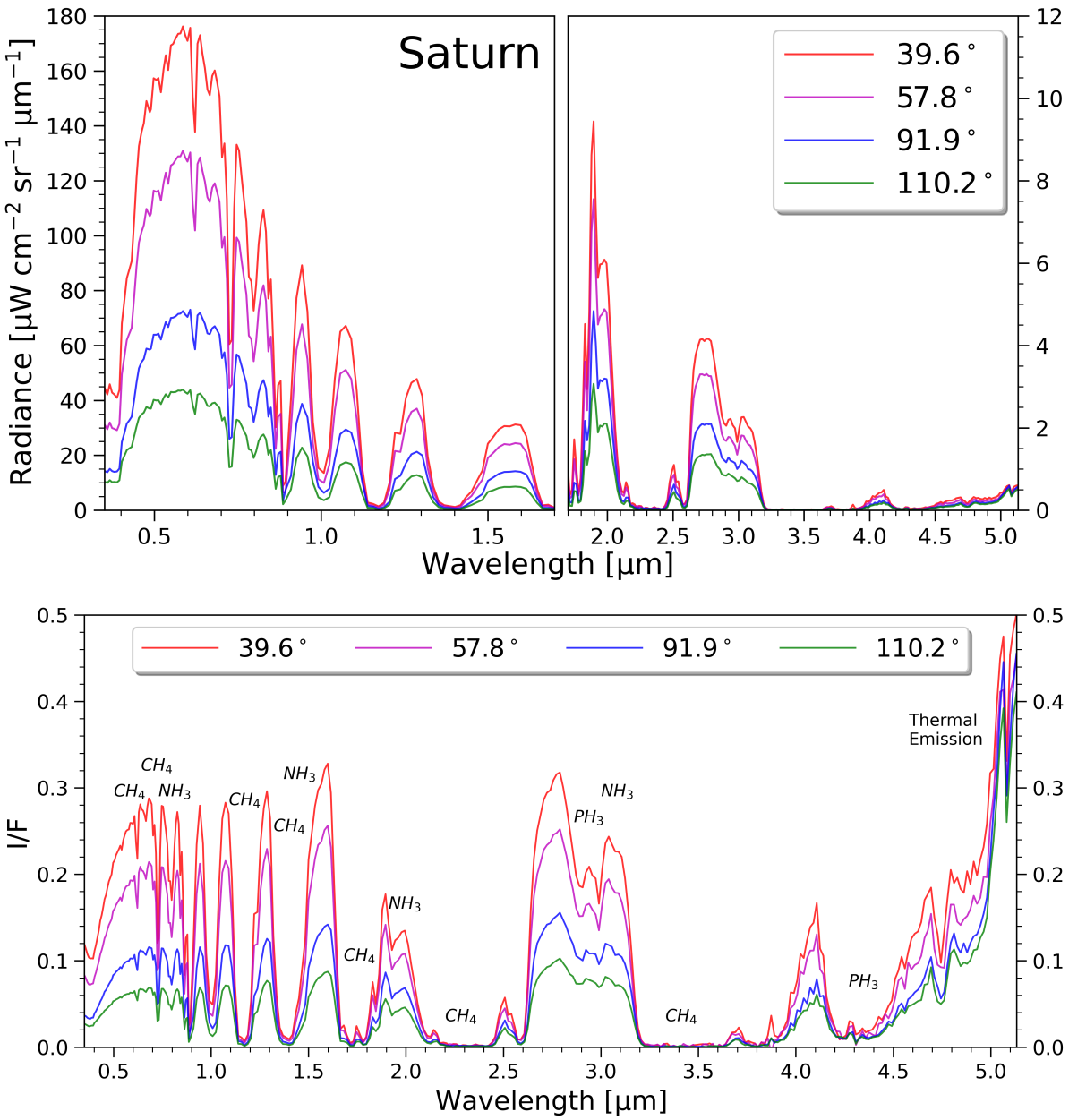

Figure 2.6: *Top*: Disk-integrated spectra of Saturn in units of flux for four phase angles ranging from 39.6° to 110.2°. Due to the nature of Cassini's orbit around Saturn, full disk, full phase spectra were impossible to obtain. *Bottom*: Same as above, but in units of I/F. Once again, prominent absorption bands, courtesy of [Vdovichenko et al., 2021] and [Baines et al., 2005], are labelled. The data used to generate this figure, as well as for two additional phase angles, can be found in the supplementary information.

inclined ring spectrum varies significantly from its ringless counterpart in the visual and near-infrared. The most significant difference is the drastic percentage-wise increase within the absorption bands. This result shows that the rings prevent the planet from appearing dark in the absorption bands, so the presence

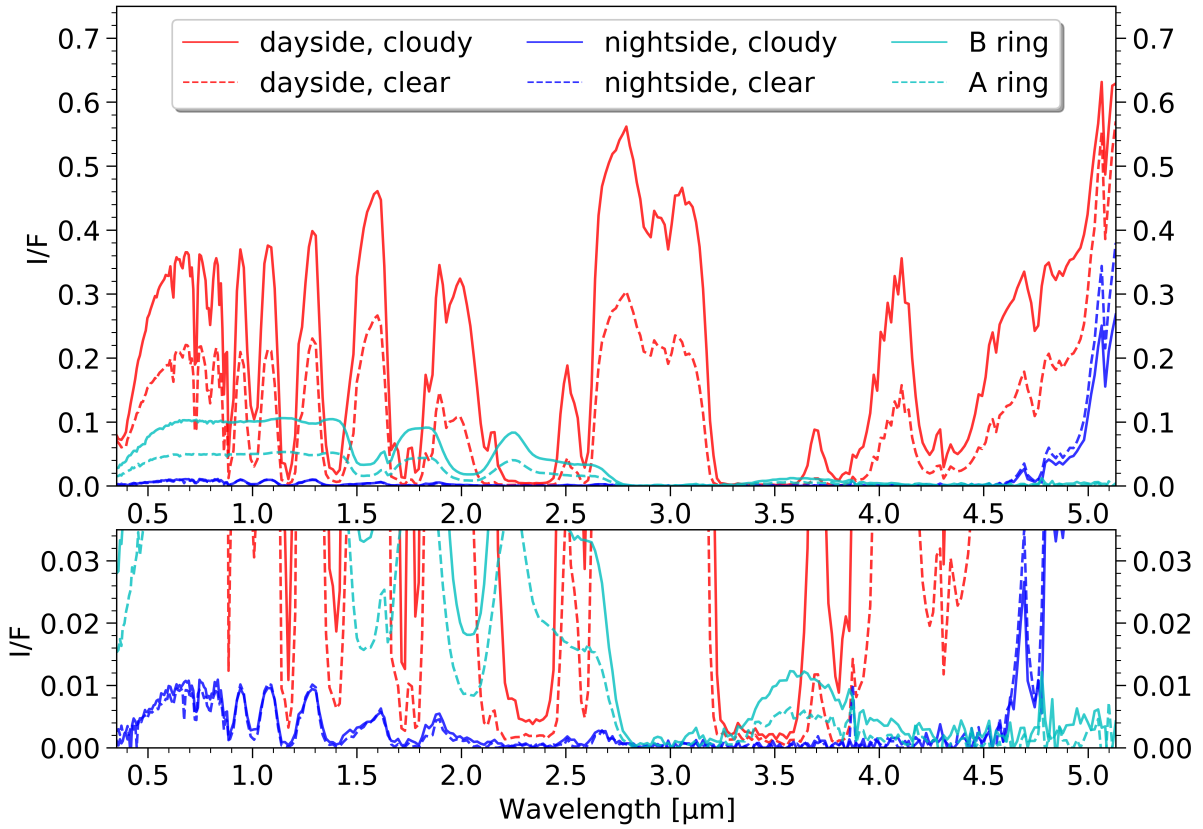

Figure 2.7: *Top*: Saturn end member spectra obtained from cube V1469259344_1 (see Figure 2.8). *Bottom*: Same as above but the y-scale has been adjusted to show detail. The features in the nightside spectra in the visible wavelengths are evidence of ringshine from Saturn's rings. The data used to generate this figure can be found in the supplementary information.

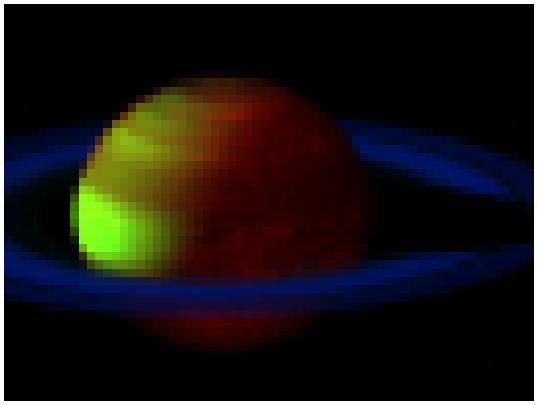

Figure 2.8: Color image of Saturn (cube V1469259344_1) with the same color mapping as in Figure 2.5: green to 2.0 μm, red to 5.0 μm, and blue to 2.4 μm.

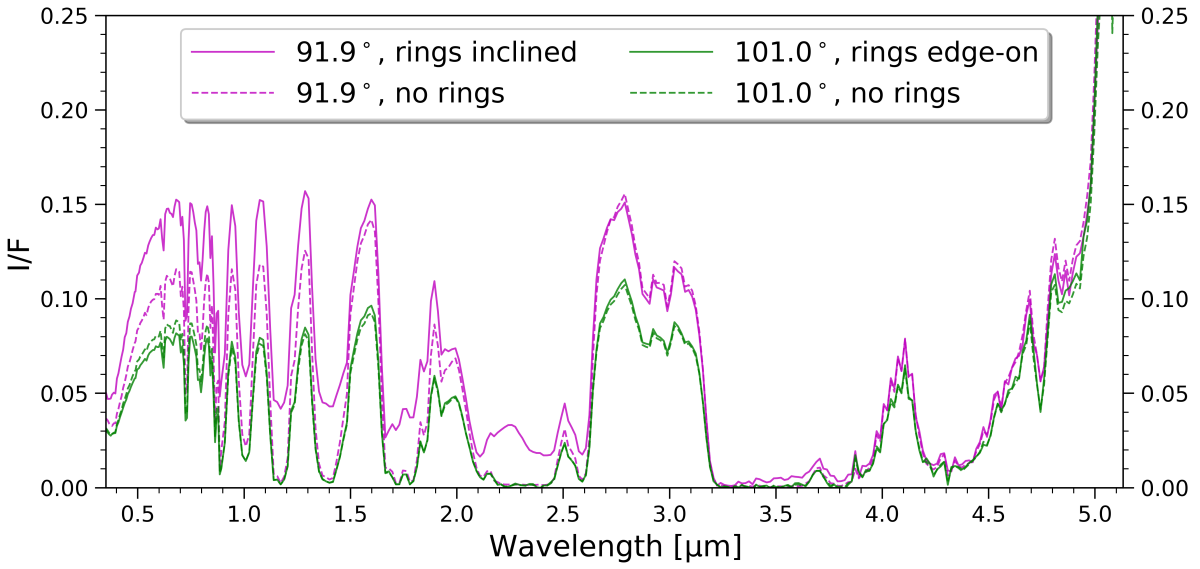

Figure 2.9: Spectral comparison of two ring geometries: edge-on rings from cube V1518276136_1 (green) and rings at an inclination of approximately 20° from cube V1469259344_1 (magenta). Spectra with the rings and their shadows removed are shown for comparison.

of water or ice can be readily observed in directly imaged brown dwarfs and exoplanets. Periodic temporal variations in spectra that oscillate between those shown in Figure 2.9 would provide strong evidence for the presence of a significant ring system.

In addition, the nightside end member spectra have minor features that resemble those in the daytime spectra (see the lower pane in Figure 2.7). We conclude that these features are evidence of the nightside being illuminated by ringshine. Such features are not present in the nightside end member spectra of Jupiter, further supporting this conclusion. While this phenomenon cannot be directly observed in exoplanets or brown dwarfs, it should be accounted for when using these spectra for comparison to models.

2.6 Conclusions

The ground truth spectral data of Jupiter and Saturn provided in this study will act as spatially resolved comparisons to distant directly imaged brown dwarfs and extrasolar gas giants. This repository of empirical data will help verify current and future atmospheric models, as well as provide a baseline for novel instruments such as the Planet as Exoplanet Analog Spectrograph (PEAS) described in [Martin et al., 2020]. Disk-integrated spectra are analogous to current direct imaging spectra and those we will obtain from future missions, while the end member spectra provide spatial context. For example, comparisons between Jupiter and Saturn show that the severity of atmospheric banding (inhomogeneities

in cloud density) in brown dwarfs and gas giants can be discerned from their mid-infrared spectra. Another interesting result is the potential to infer the presence of icy rings solely from temporal variations in point source spectra.

D. C., J. B., and J. F. are all supported by the NASA *Cassini* Data Analysis Program, grant number 80NSSC19K0897.

Chapter 3: Conclusions

In the effort to bridge the gap between the solar system and exoplanet communities, this thesis is but one step in the process. As the paper presented in Chapter 2 already has a dedicated conclusion, in this chapter I will reiterate a few key findings and discuss future projects that are extensions of this work.

Disk-integrated spectra with spatially resolved source images such as those presented in this thesis, while important, are only one piece of the puzzle. While they can help validate atmosphere models from a spatial perspective, they only provide a snapshot of a dynamic atmosphere and are unable to validate them from a temporal perspective. Therefore, the natural next step is to analyze time series disk-integrated spectra of Jupiter and Saturn. While this is a simple prospect in theory, the reality is much more complicated. As discussed in Section 2.3.1, very few cubes passed the selection criteria, and even fewer were part of a time-series set of cubes. If that wasn't problematic enough, these spectral cubes were taken in different modes (some in low-res, some in hi-res) and/or used different integration times, both introducing unnecessary sources of error. That is not to say that a temporal analysis cannot be done with VIMS data, but it would likely have to use additional techniques to overcome the issues presented here. It is my hope that future missions will learn from the mistake made with the VIMS instrument and provide much more suitable data for temporal analysis.

In addition to achieving the goals originally set forth when this project began, we encountered a few findings that were pleasant surprises. While originally thought to be a major hindrance to this project (and in many ways they were), Saturn's rings allowed us to compare the spectra of ringed and ringless planets. In our effort to synthetically remove the rings and their shadows from the Saturn cubes, we were left with the original cube and a ringless cubes, and it just so happened we had some with the rings perfectly edge-on and some with inclined rings. When plotted together (see Figure 2.9), the difference between the ringed and ringless Saturn is painfully obvious. This discovery opens up an entirely new avenue for detecting planetary rings, a notoriously difficult task, using direct imaging data. As the next generation of space telescopes provide us with a wealth of new direct imaging data, the opportunities to search for rings around those planets seems endless.

Furthermore, the methods presented in this thesis are applicable beyond their use in validating gas giant and brown dwarf atmosphere models. It has been proposed that oceans can be detected on terrestrial exoplanets by extracting signatures of specular reflection, also known as ocean glint, from exoplanet spectra [Ryan and Robinson, 2022]. Much like the models for gas giant atmospheres, the models for detecting ocean glint also need ground truth verification. During its time orbiting Saturn, *Cassini* also imaged Saturn's moon Titan extensively. Apart from Earth, Titan is the only body in the solar system

with extensive liquid lakes on its surface [Stofan et al., 2007]. *Cassini* VIMS has observed specular reflections from the lakes of Titan [Stephan et al., 2010], which would provide the ground truth needed to verify models for detecting oceans on exoplanets. Using the techniques developed for this thesis, Jason Barnes, Michael Heslar, and I began a project that would attempt to validate the claims made in [Ryan and Robinson, 2022]. As I will be completing my degree shortly, I will no longer be the lead on that project, but I intend to remain involved with it.

After completing my Masters, I will obtain certification to teach physics and math at the high school level, with the intent to teach here in Idaho.

References

[Acton, 1999] Acton, C. H. (1999). in lunar and planetary science conference. *Lunar and Planetary Science Conference*.

[Apai et al., 2017] Apai, D., Cowan, N., Kopparapu, R., Kasper, M., Hu, R., Morley, C., Fujii, Y., Kane, S., Maley, M., del Genio, A., Karalidi, T., Komacek, T., Mamajek, E., Mandell, A., Domagal-Goldman, S., Barman, T., Boss, A., Breckinridge, J., Crossfield, I., Danchi, W., Ford, E., Iro, N., Kasting, J., Lowrance, P., Madhusudhan, N., McElwain, M., Moore, W., Pascucci, I., Plavchan, P., Roberge, A., Schneider, G., Showman, A., and Turnbull, M. (2017). Exploring other worlds: Science questions for future direct imaging missions (exopag sag15 report).

[Apai et al., 2013] Apai, D., Radigan, J., Buenzli, E., Burrows, A., Reid, I. N., and Jayawardhana, R. (2013). Hst spectral mapping of l/t transition brown dwarfs reveals cloud thickness variations. *The Astrophysical Journal*, 768(2):121.

[Aumann et al., 1969] Aumann, H., Gillespie Jr, C., and Low, F. (1969). The internal powers and effective temperatures of jupiter and saturn. *The Astrophysical Journal*, 157:L69.

[Baines et al., 2005] Baines, K. H., Drossart, P., Momary, T. W., Formisano, V., Griffith, C., Bellucci, G., Bibring, J. P., Brown, R. H., Buratti, B. J., Capaccioni, F., Cerroni, P., Clark, R. N., Coradini, A., Combes, M., Cruikshank, D. P., Jaumann, R., Langevin, Y., Matson, D. L., McCord, T. B., Mennella, V., Nelson, R. M., Nicholson, P. D., Sicardy, B., and Sotin, C. (2005). The atmospheres of saturn and titan in the near-infrared: First results of cassini/vims. *Earth, Moon, and Planets*, 96:119–147.

[Barnes et al., 2013] Barnes, J. W., Clark, R. N., Sotin, C., Ádámkovics, M., Appéré, T., Rodriguez, S., Soderblom, J. M., Brown, R. H., Buratti, B. J., Baines, K. H., Le Mouélic, S., and Nicholson, P. D. (2013). A Transmission Spectrum of Titan's North Polar Atmosphere from a Specular Reflection of the Sun. ApJ, 777(2):161.

[Biller and Bonnefoy, 2018] Biller, B. A. and Bonnefoy, M. (2018). Exoplanet atmosphere measurements from direct imaging. *arXiv preprint arXiv:1807.05136*.

[Brown et al., 2004] Brown, R. H., Baines, K. H., Bellucci, G., Bibring, J.-P., Buratti, B. J., Capaccioni, F., Cerroni, P., Clark, R. N., Coradini, A., Cruikshank, D. P., et al. (2004). The cassini visual and infrared mapping spectrometer (vims) investigation. *Space Science Reviews*, 115(1-4):111–168.

[Burgasser et al., 2002] Burgasser, A. J., Kirkpatrick, J. D., Brown, M. E., Reid, I. N., Burrows, A., Liebert, J., Matthews, K., Gizis, J. E., Dahn, C. C., Monet, D. G., et al. (2002). The spectra of t dwarfs. i. near-infrared data and spectral classification. ApJ, 564(1):421.

[Burgasser et al., 2002] Burgasser, A. J., Marley, M. S., Ackerman, A. S., Saumon, D., Lodders, K., Dahn, C. C., Harris, H. C., and Kirkpatrick, J. D. (2002). Evidence of cloud disruption in the l/t dwarf transition. *The Astrophysical Journal*, 571(2):L151.

[Crossfield et al., 2014] Crossfield, I., Biller, B., Schlieder, J., Deacon, N., Bonnefoy, M., Homeier, D., Allard, F., Buenzli, E., Henning, T., Brandner, W., et al. (2014). A global cloud map of the nearest known brown dwarf. *Nature*, 505(7485):654–656.

[Cushing et al., 2011] Cushing, M. C., Kirkpatrick, J. D., Gelino, C. R., Griffith, R. L., Skrutskie, M. F., Mainzer, A., Marsh, K. A., Beichman, C. A., Burgasser, A. J., Prato, L. A., et al. (2011). The discovery of y dwarfs using data from the wide-field infrared survey explorer (wise). ApJ, 743(1):50.

[Damiano and Hu, 2020] Damiano, M. and Hu, R. (2020). Exorel: a bayesian inverse retrieval framework for exoplanetary reflected light spectra. *The Astronomical Journal*, 159(4):175.

[Damiano et al., 2020] Damiano, M., Hu, R., and Hildebrandt, S. R. (2020). Multi-orbital-phase and multiband characterization of exoplanetary atmospheres with reflected light spectra. *The Astronomical Journal*, 160(5):206.

[Fortney et al., 2020] Fortney, J. J., Visscher, C., Marley, M. S., Hood, C. E., Line, M. R., Thorngren, D. P., Freedman, R. S., and Lupu, R. (2020). Beyond equilibrium temperature: How the atmosphere/interior connection affects the onset of methane, ammonia, and clouds in warm transiting giant planets. *The Astronomical Journal*, 160(6):288.

[Gu et al., 2021] Gu, L., Fan, S., Li, J., Bartlett, S. J., Natraj, V., Jiang, J. H., Crisp, D., Hu, Y., Tinetti, G., and Yung, Y. L. (2021). Earth as a proxy exoplanet: Deconstructing and reconstructing spectrophotometric light curves. *The Astronomical Journal*, 161(3):122.

[Kirkpatrick et al., 1999] Kirkpatrick, J. D., Reid, I. N., Liebert, J., Cutri, R. M., Nelson, B., Beichman, C. A., Dahn, C. C., Monet, D. G., Gizis, J. E., and Skrutskie, M. F. (1999). Dwarfs cooler than âmâ: The definition of spectral type âlâ using discoveries from the 2-micron all-sky survey (2mass). ApJ, 519(2):802.

[Lew et al., 2020] Lew, B. W., Apai, D., Marley, M., Saumon, D., Schneider, G., Zhou, Y., Cowan, N. B., Karalidi, T., Manjavacas, E., Bedin, L., et al. (2020). Cloud atlas: Unraveling the vertical cloud

structure with the time-series spectrophotometry of an unusually red brown dwarf. *The Astrophysical Journal*, 903(1):15.

[Luhman, 2014] Luhman, K. L. (2014). Discovery of a 250 k brown dwarf at 2 pc from the sun. ApJ, 786(2):L18.

[Lupu et al., 2016] Lupu, R. E., Marley, M. S., Lewis, N., Line, M., Traub, W. A., and Zahnle, K. (2016). Developing atmospheric retrieval methods for direct imaging spectroscopy of gas giants in reflected light. i. methane abundances and basic cloud properties. *The Astronomical Journal*, 152(6):217.

[MacDonald et al., 2018] MacDonald, R. J., Marley, M. S., Fortney, J. J., and Lewis, N. K. (2018). Exploring h2o prominence in reflection spectra of cool giant planets. *The Astrophysical Journal*, 858(2):69.

[Marley et al., 1999] Marley, M. S., Gelino, C., Stephens, D., Lunine, J. I., and Freedman, R. (1999). Reflected spectra and albedos of extrasolar giant planets. i. clear and cloudy atmospheres. *The Astrophysical Journal*, 513(2):879.

[Marley et al., 2010] Marley, M. S., Saumon, D., and Goldblatt, C. (2010). A patchy cloud model for the l to t dwarf transition. ApJ, 723(1):L117.

[Martin et al., 2020] Martin, E. C., Skemer, A. J., Radovan, M. V., Allen, S. L., Black, D., Deich, W. T., Fortney, J. J., Kruglikov, G., MacDonald, N., Marques, D., et al. (2020). The planet as exoplanet analog spectrograph (peas): design and first-light. 11447:135–143.

[Mayor and Queloz, 1995] Mayor, M. and Queloz, D. (1995). A jupiter-mass companion to a solar-type star. *Nature*, 378:355–359.

[Metchev et al., 2015] Metchev, S. A., Heinze, A., Apai, D., Flateau, D., Radigan, J., Burgasser, A., Marley, M. S., Artigau, É., Plavchan, P., and Goldman, B. (2015). Weather on other worlds. ii. survey results: Spots are ubiquitous on l and t dwarfs. *The Astrophysical Journal*, 799(2):154.

[National Academies of Sciences et al., 2021] National Academies of Sciences, E., Medicine, et al. (2021). Pathways to discovery in astronomy and astrophysics for the 2020s.

[Nayak et al., 2017] Nayak, M., Lupu, R., Marley, M. S., Fortney, J. J., Robinson, T., and Lewis, N. (2017). Atmospheric retrieval for direct imaging spectroscopy of gas giants in reflected light. ii. orbital phase and planetary radius. *Publications of the Astronomical Society of the Pacific*, 129(973):034401.

[Ryan and Robinson, 2022] Ryan, D. J. and Robinson, T. D. (2022). Detecting oceans on exoplanets with phase-dependent spectral principal component analysis. *The Planetary Science Journal*, 3(2):33.

[Simon et al., 2016] Simon, A. A., Rowe, J. F., Gaulme, P., Hammel, H. B., Casewell, S. L., Fortney, J. J., Gizis, J. E., Lissauer, J. J., Morales-Juberias, R., Orton, G. S., et al. (2016). Neptuneâs dynamic atmosphere from kepler k2 observations: implications for brown dwarf light curve analyses. *The Astrophysical Journal*, 817(2):162.

[Stephan et al., 2010] Stephan, K., Jaumann, R., Brown, R. H., Soderblom, J. M., Soderblom, L. A., Barnes, J. W., Sotin, C., Griffith, C. A., Kirk, R. L., Baines, K. H., et al. (2010). Specular reflection on titan: liquids in kraken mare. *Geophysical Research Letters*, 37(7).

[Stofan et al., 2007] Stofan, E. R., Elachi, C., Lunine, J. I., Lorenz, R. D., Stiles, B., Mitchell, K., Ostro, S., Soderblom, L., Wood, C., Zebker, H., et al. (2007). The lakes of titan. *Nature*, 445(7123):61–64.

[Sudarsky et al., 2003] Sudarsky, D., Burrows, A., and Hubeny, I. (2003). Theoretical spectra and atmospheres of extrasolar giant planets. *The Astrophysical Journal*, 588(2):1121.

[Sudarsky et al., 2000] Sudarsky, D., Burrows, A., and Pinto, P. (2000). Albedo and reflection spectra of extrasolar giant planets. *The Astrophysical Journal*, 538(2):885.

[Traub and Oppenheimer, 2010] Traub, W. A. and Oppenheimer, B. R. (2010). Direct imaging of exoplanets. *Exoplanets*, pages 111–156.

[Vdovichenko et al., 2021] Vdovichenko, V. D., Karimov, A. M., Kirienko, G. A., Lysenko, P. G., Tejfel, V. G., Filippov, V. A., Kharitonova, G. A., and Khozhenets, A. P. (2021). Zonal features in the behavior of weak molecular absorption bands on jupiter. *Solar System Research*, 55:35–46.

[Zhou et al., 2016] Zhou, Y., Apai, D., Schneider, G. H., Marley, M. S., and Showman, A. P. (2016). Discovery of rotational modulations in the planetary-mass companion 2m1207b: intermediate rotation period and heterogeneous clouds in a low gravity atmosphere. *The Astrophysical Journal*, 818(2):176.